Electronic Supplementary Information

In-Situ Embedding of Cobaltous Sulfide Quantum Dots among Transition Metal Layered Double Hydroxide for High Performance All-Solid-State Asymmetric Supercapacitors

Zhiqiang Liu[a, 1], Yanling Qiu[a, 1], Aitang Zhang[a], Wenrong Yang[b], Colin J. Barrow[b], Joselito M. Razal[c], Jingquan Liu[a*]

[a]*College of Materials Science and Engineering, Institute for Graphene Applied Technology Innovation, Qingdao University, Qingdao, 266071, China.*

[b]*School of Life and Environmental Sciences, Institute for Frontier Materials, Deakin University, Geelong, VIC 3216, Australia.*

[c]*Institute for Frontier Materials, Deakin University, Geelong, VIC 3216, Australia.*

*Corresponding authors.

Tel: +86 532 83780128.

E-mails: jliu@qdu.edu.cn (Jingquan Liu)

[1]Zhiqiang Liu and Yanling Qiu contributed equally to this work.

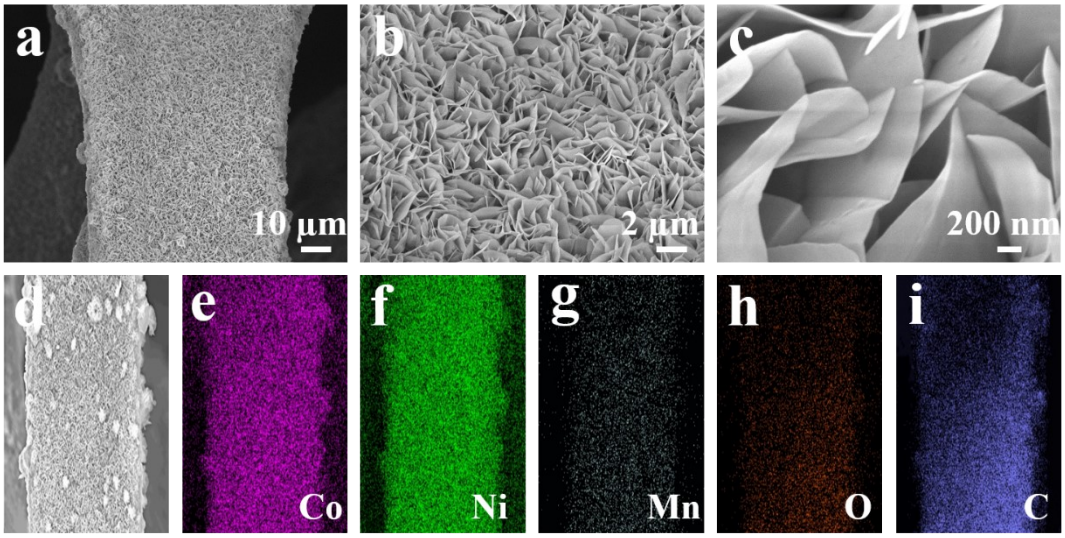

Figure S1. SEM micrographs of (a-c) Ni_1Mn_3Co-LDH/NF at different magnifications, (d-i) EDS elemental mapping images of Ni_1Mn_3Co-LDH/NF.

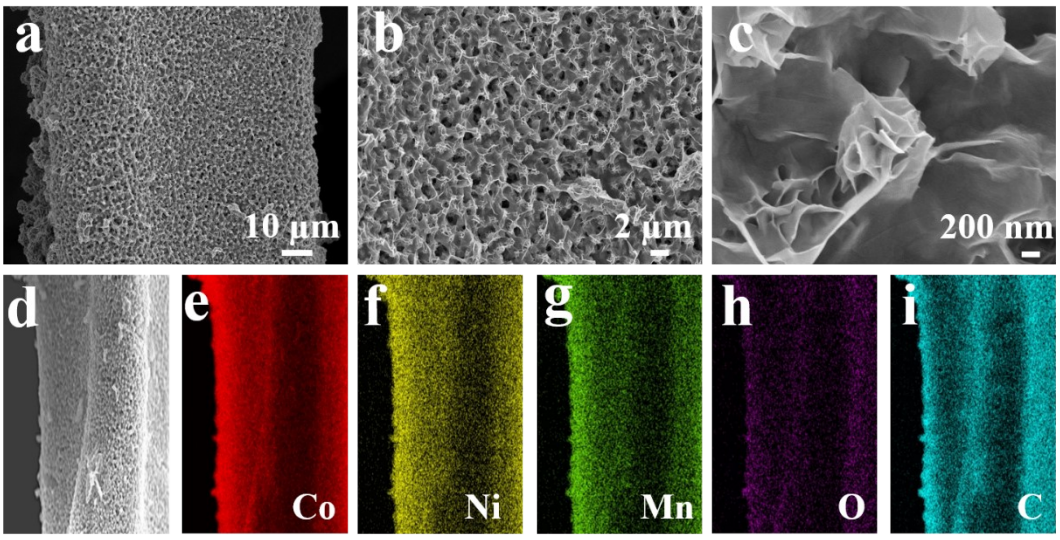

Figure S2. SEM micrographs of (a-c) Ni_2Mn_2Co-LDH/NF at different magnifications, (d-i) EDS elemental mapping images of Ni_2Mn_2Co-LDH/NF.

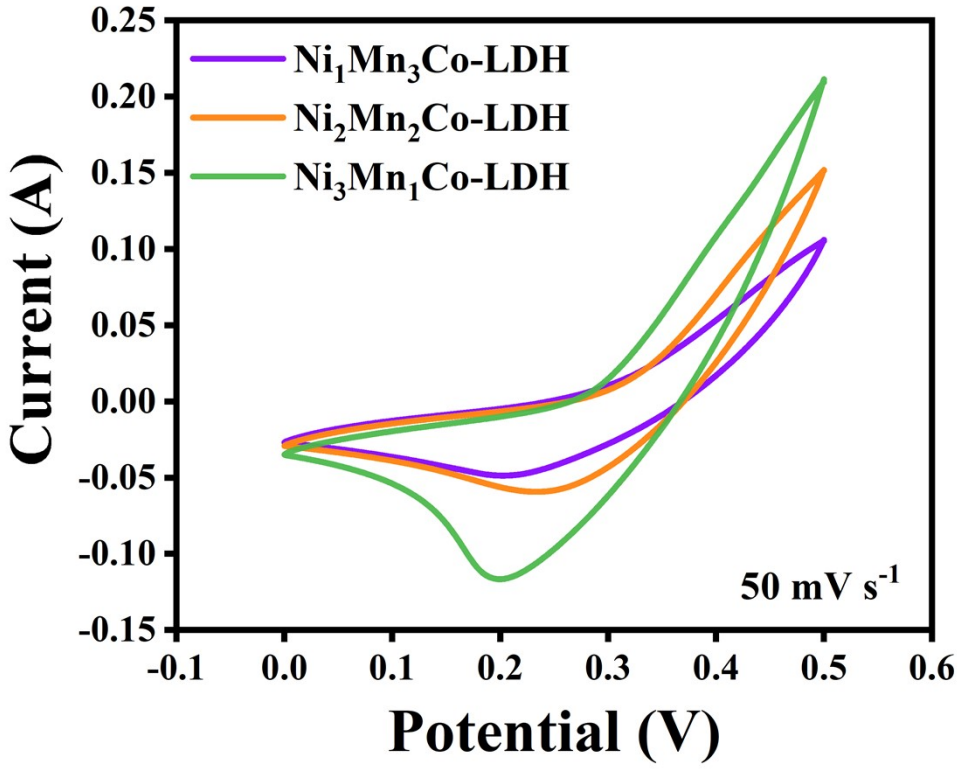

Figure S3. CV curves of $Ni_xMn_{4-x}Co$-LDH composited with various Ni/Co ratios at

50 mV s^{-1}.

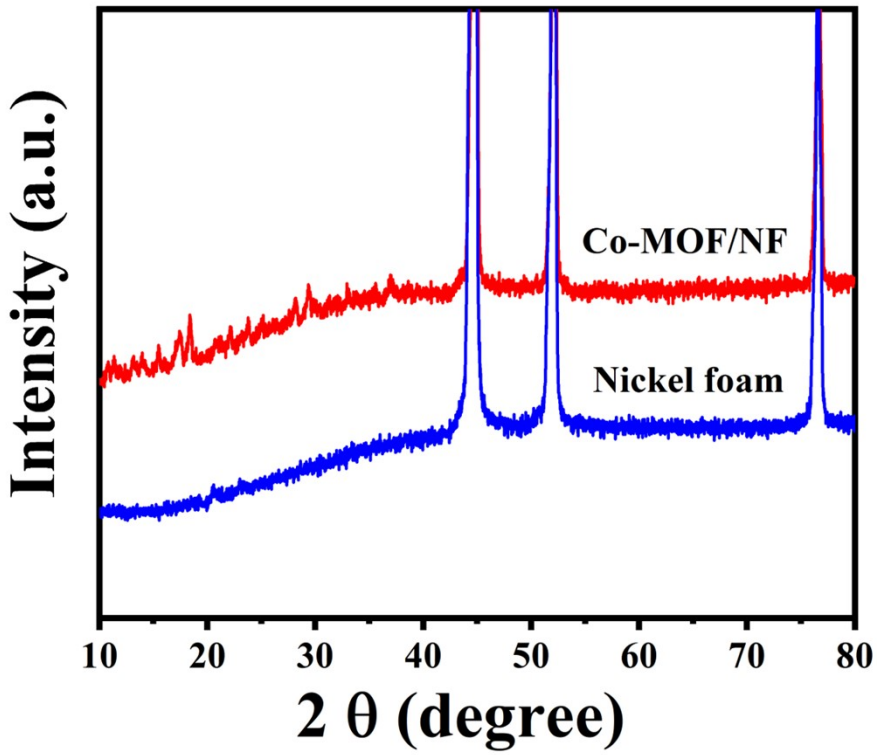

Figure S4. XRD patterns of the Co-MOF and nickel foam.

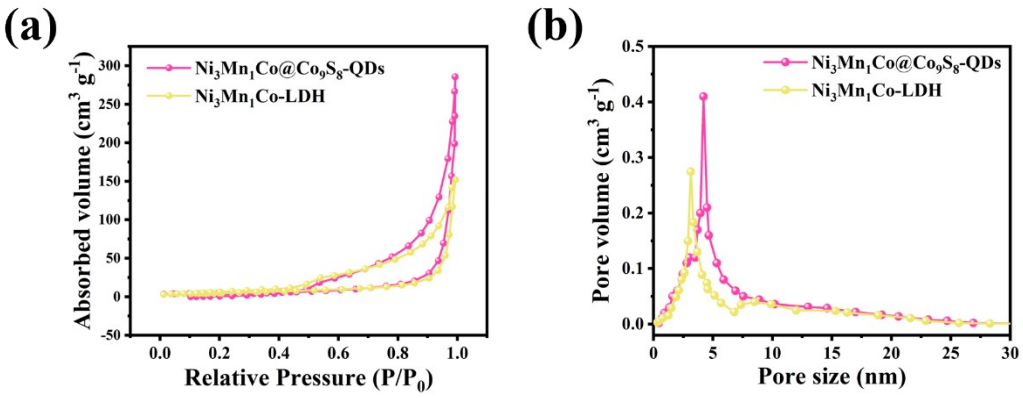

Figure S5. (a) N_2 adsorption-desorption isotherms and (b) pore size distribution patterns of Ni_3Mn_1Co-LDH/NF and $Ni_3Mn_1Co@Co_9S_8$-QDs/NF.

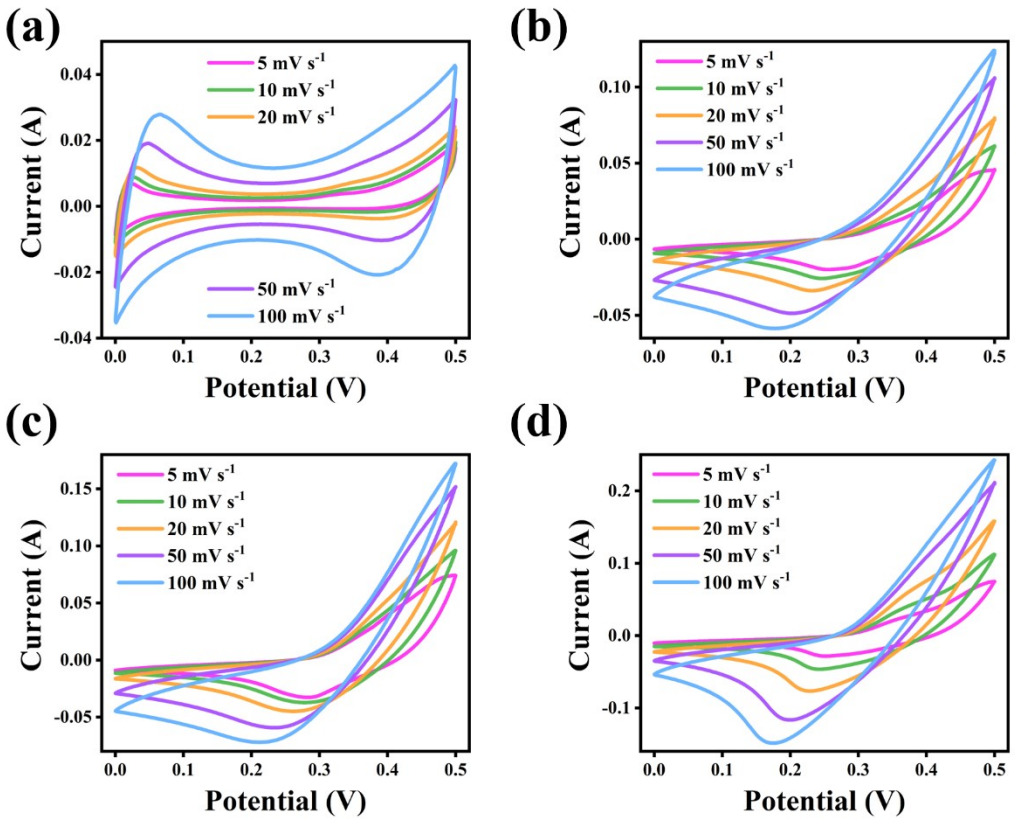

Figure S6. CV curves of the (a) Co-MOF/NF and (b) Ni_1Mn_3Co-LDH/NF and (c) Ni_2Mn_2Co-LDH/NF and (d) Ni_3Mn_1Co-LDH/NF electrode at different scan rates ranging from 5 to 100 mV s^{-1}.

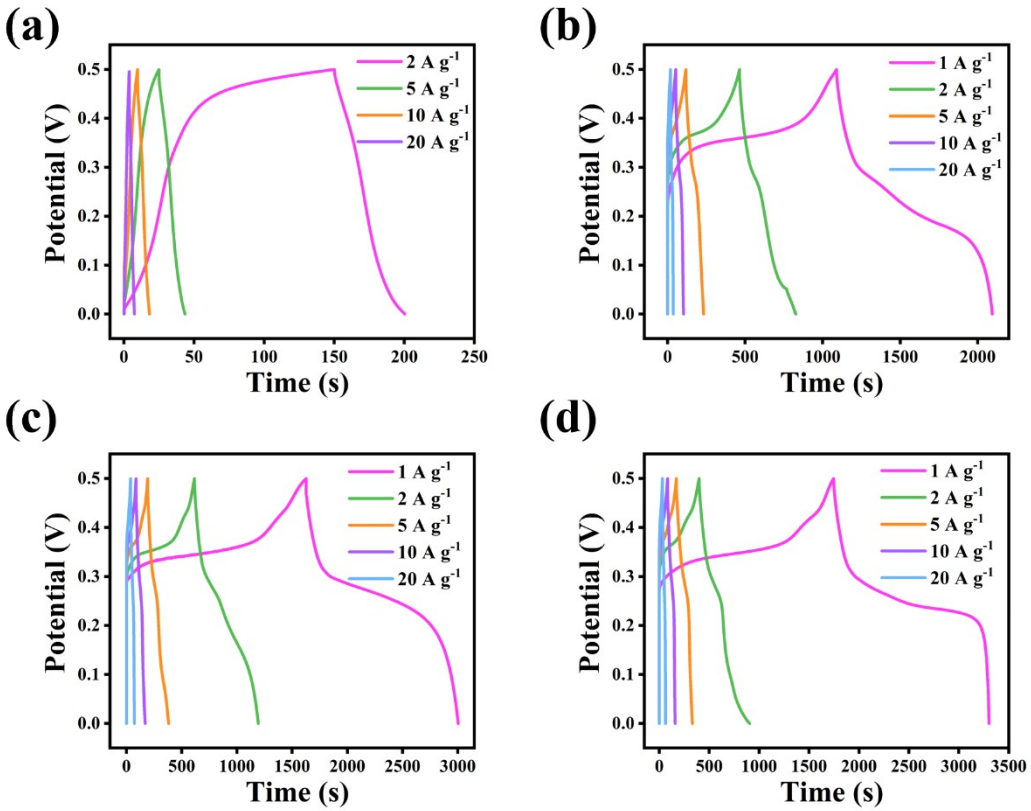

Figure S7. GCD curves of the (a) Co-MOF/NF and (b) Ni_1Mn_3Co-LDH/NF and (c) Ni_2Mn_2Co-LDH/NF and (d) Ni_3Mn_1Co-LDH/NF electrode at different current densities ranging from 1 to 20 A g^{-1}.

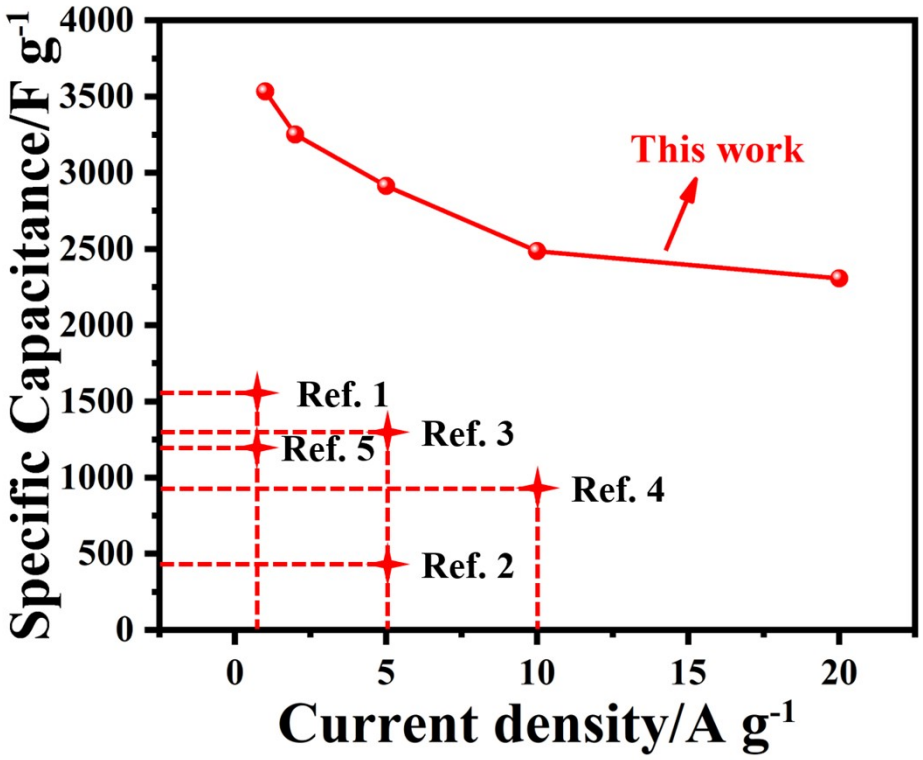

Figure S8. A comparison of the specific capacitances of our $Ni_3Mn_1Co@Co_9S_8$-QDs/NF electrode with those previously reported cobalt sulfide electrode materials.

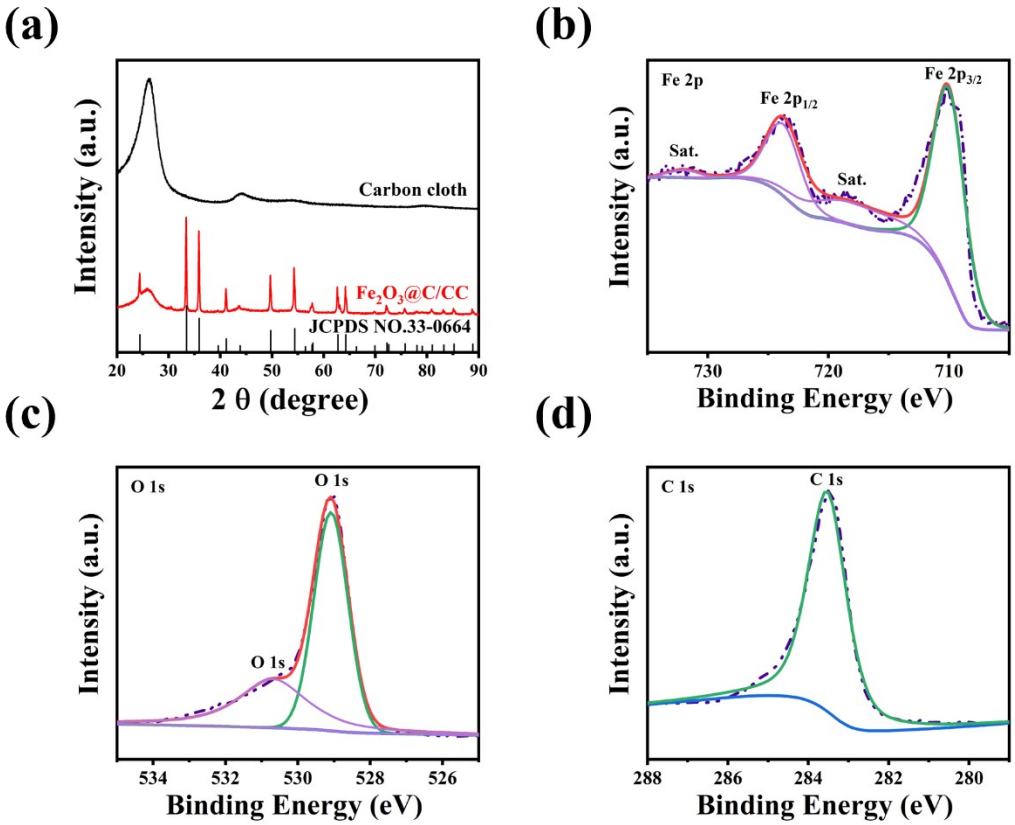

Figure S9. (a) XRD patterns of the Fe_2O_3@C/CC. The narrow spectra of (b) Fe 2p, (c) O 1s and (d) C 1s for Fe_2O_3@C/CC.

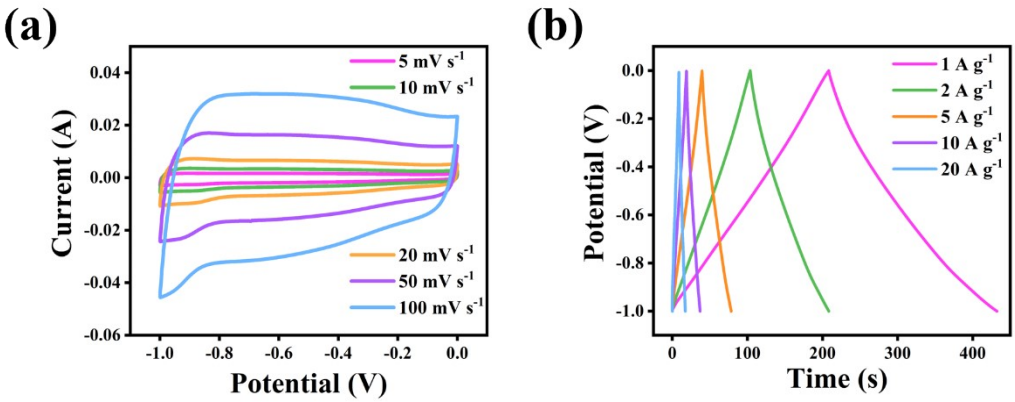

Figure S10. (a) CV curves of the Fe_2O_3@C/CC electrode at different scan rates ranging from 5 to 100 mV s^{-1} (b) GCD curves of the Fe_2O_3@C/CC electrode at different current densities ranging from 1 to 20 A g^{-1}.

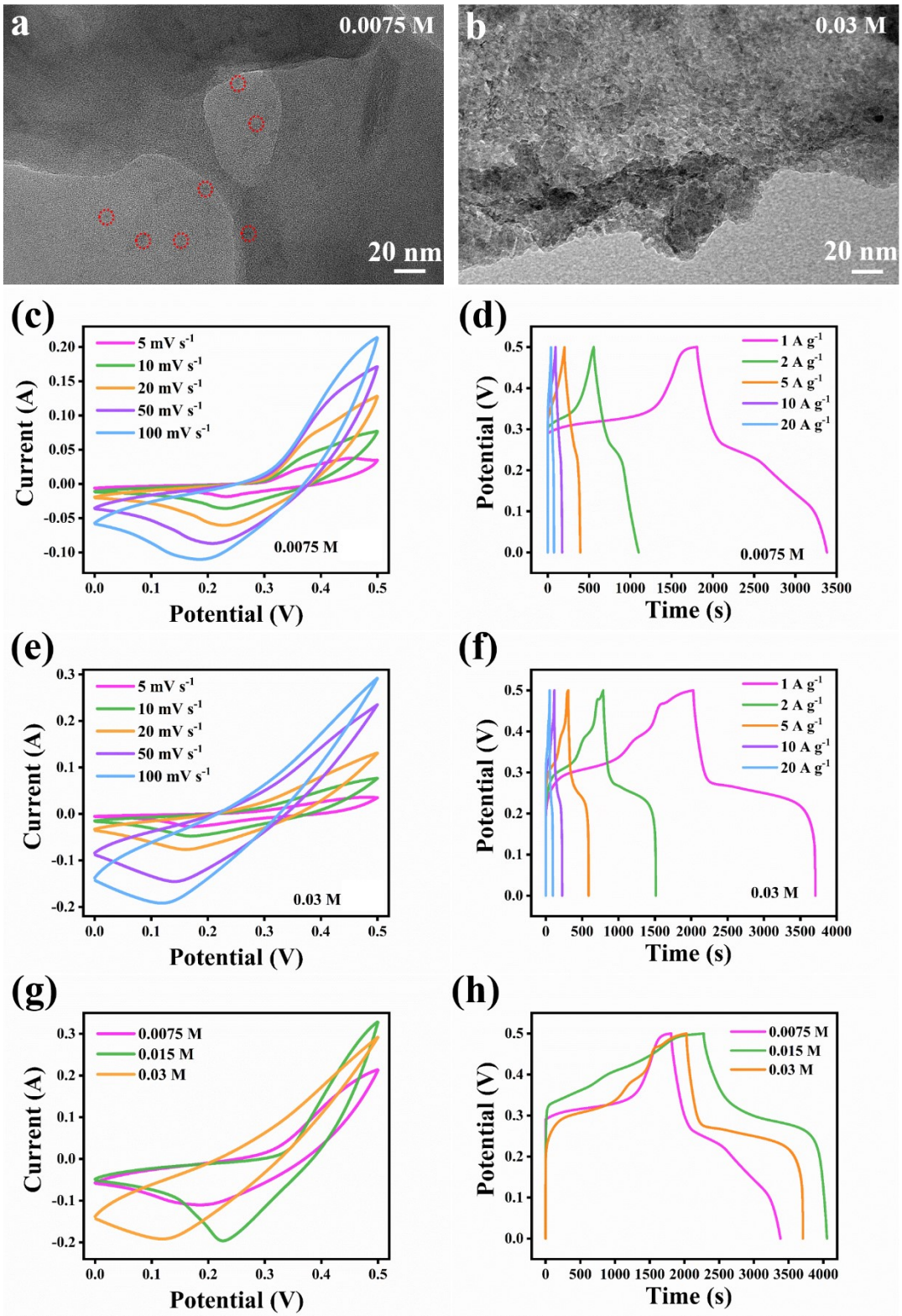
a
0.0075 M
20 nm
b
0.03 M
20 nm
(c)
5 mV s-1
10 mV s-1
20 mV s-1
50 mV s-1
100 mV s-1
0.0075 M
Current (A)
Potential (V)
(d)
1 A g-1
2 A g-1
5 A g-1
10 A g-1
20 A g-1
0.0075 M
Potential (V)
Time (s)
(e)
5 mV s-1
10 mV s-1
20 mV s-1
50 mV s-1
100 mV s-1
0.03 M
Current (A)
Potential (V)
(f)
1 A g-1
2 A g-1
5 A g-1
10 A g-1
20 A g-1
0.03 M
Potential (V)
Time (s)
(g)
0.0075 M
0.015 M
0.03 M
Current (A)
Potential (V)
(h)
0.0075 M
0.015 M
0.03 M
Potential (V)
Time (s)

Figure S11 (a, b) TEM images of Co_9S_8-QDs synthesized from different concentrations of TAA (c-h) CV and GCD curves of Co_9S_8-QDs synthesized from different concentrations of TAA.

Active material	Electrolyte	Capacitance	Energy density	Ref.
$Ni_3Mn_1Co@Co_9S_8$-QDs/NF	6 M KOH	492.1 mAh g^{-1} (3534 F g^{-1}) at 1 A g^{-1}	71.48 Wh kg^{-1}	This work
CoS-NiO	3 M KCl	1527 F g^{-1} at 1 A g^{-1}	39 Wh kg^{-1}	[1]
Co_3O_4/CoS NSs	2 M KOH	1658 F g^{-1} at 1 A g^{-1}	23.6 Wh kg^{-1}	[4]
5-NiS@CoS	2 M KOH	1210 F g^{-1} at 1 A g^{-1}	24.1 Wh kg^{-1}	[5]
KCu_7S_4@NiMn LDHs	1 M LiOH	879 F g^{-1} at 1 mV s^{-1}	15.9 Wh kg^{-1}	[6]
CC@NiCo-LDH/Co_9S_8	6 M KOH	2438 F g^{-1} at 5 A g^{-1}	38 Wh kg^{-1}	[7]
MC@CF-LDH-3	6 M KOH	903.15 C g^{-1} at 1 A g^{-1}	60.82 Wh kg^{-1}	[8]
NiCoP/NiCo-OH30	3 M KOH	1100 F g^{-1} at 1 A g^{-1}	34 Wh kg^{-1}	[9]

Table S1 Compared the performances reported in our work and those recently reported on LDHs and cobalt sulfide related materials for supercapacitors.

References

[1] V. Kumbhar, H. Lee, J. Lee, N. Chodankar and K. Lee, *J. Alloy. Compd.,* 2021, **863,** 158064.

[2] J. Jiang, J. Xu, W. Wang, L. Zhang and G. Xu, *Chemistry,* 2020, **26,** 14903-14911.

[3] M. Chuai, H. Zhang, Y. Tong, K. Zhang and M. Zhang, *Sustain. Energy. Fuels,* 2020, **4,** 3511-3518.

[4] Y. Lu, W. Yang, W. Li, M. Chen, L. Shuai, P. Qi, D. Zhang, H. Du, Y. Tang and M. Qiu, *J. Alloy. Compd.,* 2020, **818,** 152877.

[5] Y. Miao, X. Zhang, J. Zhan, Y. Sui, J. Qi, F. Wei, Q. Meng, Y. He, Y. Ren, Z. Zhan and Z. Sun, *Adv, Mater, Inter.,* 2019, **7,** 1901618.

[6] X. Guo, J. Zhang, W. Xu, C. Hu, L. Sun and Y. Zhang, *J. Mater. Chem. A*, 2017, 5, 20579-20587.

[7] Q. Yang, Y. Liu, L. Xiao, M. Yan, H. Bai, F. Zhu, Y. Lei and W. Shi, *Chem. Eng. J.,* 2018, **354,** 716-726.

[8] Z. Liu, Y. Liu, Y. Zhong L., Cui, W. Yang, J. M. Razal, C. J. Barrow and J. Liu, *J. Power Sources,* 2021, **484,** 229288.

[9] X. Li, H. Wu, A. Elshahawy, L. Wang, S. Pennycook, C. Guan and J. Wang, *Adv. Funct. Mater.,* 2018, **28,** 1800036.